EXPRESS LETTER

Upward propagation of gravity waves and ionospheric perturbations triggered by the 2022 Hunga-Tonga volcanic eruption

Yasunobu Miyoshi[1][*] and Hiroyuki Shinagawa[2]

Abstract

Using an atmosphere–ionosphere coupled model (GAIA), atmospheric and ionospheric perturbations triggered by the 2022 Hunga-Tonga volcanic eruption are studied. Our result shows that ionospheric perturbations are caused by neutral wind perturbations associated with gravity waves. Gravity waves with horizontal phase speeds of 200–310 m/s are excited in the troposphere near the Hunga-Tonga volcano, and propagate upward into the thermosphere. While the amplitude of the eruption-generated gravity waves is small in the troposphere (~ 1 m/s), the amplitude of the gravity waves increases exponentially with height because of the exponential decrease of the density, reaching 60–80 m/s at 300 km height. General features of the TIDs appeared in GNSS–TEC observations reported in earlier studies are reproduced fairly well. We can conclude that the eruption-generated gravity waves whose horizontal phase velocity is close to the sound speed play an important role in thermospheric and ionospheric perturbations after the Hunga-Tonga volcano eruption.

Keywords 2022 Hunga Tonga–Hunga Ha, Apai volcanic eruption, Gravity wave, GNSS–TEC variation
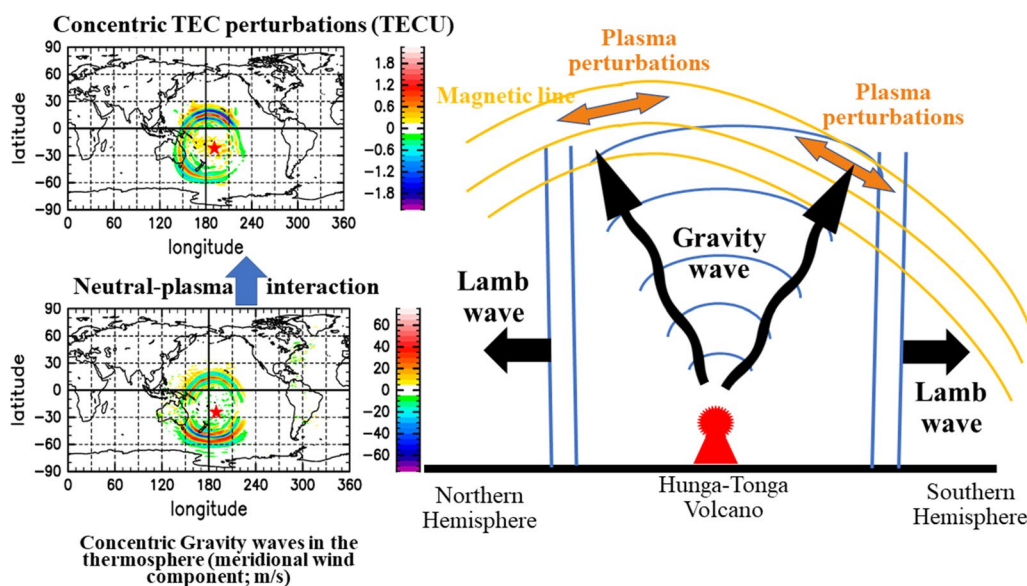
*Correspondence:
Yasunobu Miyoshi
miyoshi.yasunobu.527@m.kyushu-u.ac.jp
Full list of author information is available at the end of the article

Graphical Abstract

Introduction

On 15th January 2022 the Hunga Tonga-Hunga Ha'apai volcano (20.05° S, 175.4° W) erupted at about 04:15 UT. Large-amplitude Lamb waves which appeared to be related to the eruption were observed at many stations worldwide (Amores et al. 2022; Matoza et al. 2022; Abbrescia et al. 2022; Harding et al. 2022; Kubo et al. 2022; Yamada et al. 2022). In addition to Lamb waves, which travel with a speed of about 310 m/s, some signatures of acoustic waves and atmospheric gravity waves (GWs) were also detected (Themens et al. 2022; Adam 2022; Heki 2022; Iyemori et al. 2022; Yamazaki et al. 2022). Those waves are likely to propagate upward to the upper atmosphere, producing electron density perturbations in the ionosphere. Indeed, traveling ionospheric disturbances (TIDs) were detected by the analysis of total electron content (TEC), which are likely to be caused by the atmospheric waves (Astafyeva et al. 2022; Lin et al. 2022; Saito 2022; Themens et al. 2022). The TIDs arrived at Australia at 7–8 UT, and at Japan at 11–12 UT. There are also some reports that the first TID arrived at Japan at 7–8 UT which is about 3 h before the arrival of the Lamb wave front (Saito 2022; Shinbori et al. 2022; Lin et al. 2022). This phenomenon was interpreted as the effect of electric fields transmitted along magnetic field lines from the geomagnetic conjugate in the southern hemisphere (SH), where the dynamo electric field is generated by the eruption-generated atmospheric waves in the E-region. However, there have been no global model simulations concerning ionospheric perturbation triggered by the 2022 Hunga-Tonga eruption. In this study, for the first time, we show analysis of atmospheric and ionospheric perturbations associated with the Hunga-Tonga volcanic eruption using a global atmosphere–ionosphere coupled model GAIA (Ground-to-topside of Atmosphere and Ionosphere for Aeronomy). Numerical studies concerning the impact of the Hunga-Tonga eruption with other numerical models are underway, and will be published shortly. Although GAIA is a hydrostatic model that is not able to generate acoustic waves, the model is capable of reproducing Lamb waves and GWs. Therefore, some features of the ionospheric disturbances caused by Lamb waves and GWs can be reproduced using the model.

Description of the model and numerical simulation

GAIA is a global atmosphere–ionosphere coupled model, which contains all atmospheric regions from the ground surface to the upper thermosphere/ionosphere (Jin et al. 2011). To study Lamb/GWs associated with the Hunga-Tonga volcanic eruption, and their impacts on the ionosphere, GAIA with a higher horizontal resolution is used (Miyoshi et al. 2018). Details of GAIA can be found in Jin et al. (2011, 2012). For the neutral atmospheric part of GAIA, a whole atmosphere General Circulation Model (GCM) is used (Miyoshi and Fujiwara 2003, 2006; Miyoshi and Yamazaki 2020). The GCM is a global model with a horizontal resolution of approximately 1° longitude by 1° latitude. The vertical resolution

is 0.2 scale heights. The GCM includes a full set of physical processes, such as solar and infrared radiation, moist convection, boundary layer, molecular and thermal viscosity, Joule heating, and ion-drag force. Furthermore, meteorological reanalysis data provided by Japan Meteorological Agency (JRA55) are incorporated below 40 km height by a nudging method (Kobayashi et al. 2015). This means that the GCM can simulate realistic temporal and spatial variations in the lower atmosphere on the day of the Hunga-Tonga volcanic eruption. For the ionospheric part of GAIA, ionosphere model developed by Shinagawa (2009) is used. The coupling process between the neutrals and ionospheric plasmas are calculated by including collisional and chemical coupling as well as electrodynamical coupling. The electrodynamics model is also incorporated (Jin et al. 2008) to calculate the global distribution of the ionospheric current and electric fields. The tilted dipole of the geomagnetic configuration and the condition of equipotentiality along the geomagnetic field lines. This means that this model can simulate an electromagnetic coupling process via the geomagnetic field line between the hemispheres. The horizonal and vertical resolutions of the ionosphere model are 1° longitude by 1° latitude and 10 km height, respectively. GAIA can simulate waves/disturbances with horizontal wavelength longer than about 400 km. However, it is noted that GAIA is unable to simulate acoustic waves and their impact on the ionosphere, because GAIA is a hydrostatic model.

To investigate atmospheric and ionospheric perturbations triggered by the Hunga-Tonga eruption, we conducted two kinds of numerical simulations. The first is a simulation without the eruption (CNTL). The other is a simulation with the eruption (EXP). In the EXP, the initial perturbation generated by the eruption is given by adding a surface pressure perturbation of $+4$ hPa at a grid point near the Hunga-Tonga during a period from 04:00 UT to 04:30 UT on 15 January 2022, because a surface perturbation of about 4 hPa was observed near the Hunga-Tonga volcano (Yamada et al. 2022). This surface pressure perturbation excites the pressure, temperature, and wind perturbations in the troposphere near the Hunga-Tonga volcano. The intensity and time evolution of the initial perturbation are chosen to reproduce the observed TEC variation. It is noted that the intensity of the initial perturbation has some uncertainties. In other words, if the intensity of the initial perturbation increased, simulated waves and TEC variations were enhanced.

In this study, geomagnetically quiet condition was assumed during the numerical simulation. In the real atmosphere, a weak geomagnetic disturbance with $K_p = 3 - 4$ occurred during the eruption. The influence of the geomagnetic activity during the Hunga-Tonga

eruption was studied by He et al. (2023). He et al. (2023) indicated that the propagation direction of the observed TIDs is different from that generated by the geomagnetic storm. The TEC variations observed by Saito (2022) are filtered perturbations with certain band of periodicity (typically a few 10 s minutes to 1 h). For perturbations with different time scale, the magnetic storm effects may not necessarily be ignored. The storm effects would be small for the observed TIDs, although further studies concerning the storm effect on the observed TIDs are necessary. F10.7 cm flux was used as a proxy for the solar UV/EUV fluxes, and was set to 111.6×10^{-22} and $119.4 \times 10^{-22} \mathrm{Wm}^{-2}\mathrm{Hz}^{-1}$ on 15 January and 16 January, respectively. Numerical simulation was conducted during a period from 00 UT 15 January 2022 to 00 UT 17 January 2022. Data were sampled every 5 min. The atmospheric and ionospheric perturbations triggered by the Hunga-Tonga eruption are excluded in the simulation without the eruption (CNTL), while an initial surface pressure perturbation is considered in the simulation with the eruption (EXP). By taking the difference between with and without the eruption, we can elucidate perturbations triggered by the Hunga-Tonga eruption, their upward propagation, and their impact on the T–I system. For example, taking the difference of the simulated TEC variations between with and without the eruption at each time step, the TEC variations triggered by the Hunga-Tonga eruption will be shown.

Additional file 1: Figure S1 shows the zonal mean temperature and zonal wind on 15 January obtained by CNTL. The eastward and westward strato-mesospheric jets are located in middle and high latitudes in the northern hemisphere (NH) and SH, respectively. The weak zonal wind region appears near the mesopause. Additional file 1: Figure S2 shows the global distributions of the horizontal wind and temperature at 300 km height at 04 UT, 06UT, and 08UT. Note that the horizontal wind near the Hunga-Tonga volcano is weak eastward during the eruption (04 UT), while strong north-eastward wind (200–300 m/s) prevails after the eruption (06–08 UT).

Results

Figure 1 shows the global distributions of TEC variation triggered by the Hunga-Tonga eruption (Animation of TEC variation triggered by the Hunga-Tonga eruption is shown in Additional file 2). The TEC variations with the amplitude of 1 TECU appear over New Zealand and equatorial Pacific at 06 UT and reach over Australia at 07 UT. The concentric wave pattern of the TEC variations is clear at 07 UT and 08 UT, and is distorted after 10 UT. The TEC variations reach Antarctica at 10 UT and Atlantic Ocean at 12 UT. These features of the simulated TEC variations are quite similar to those of the observations
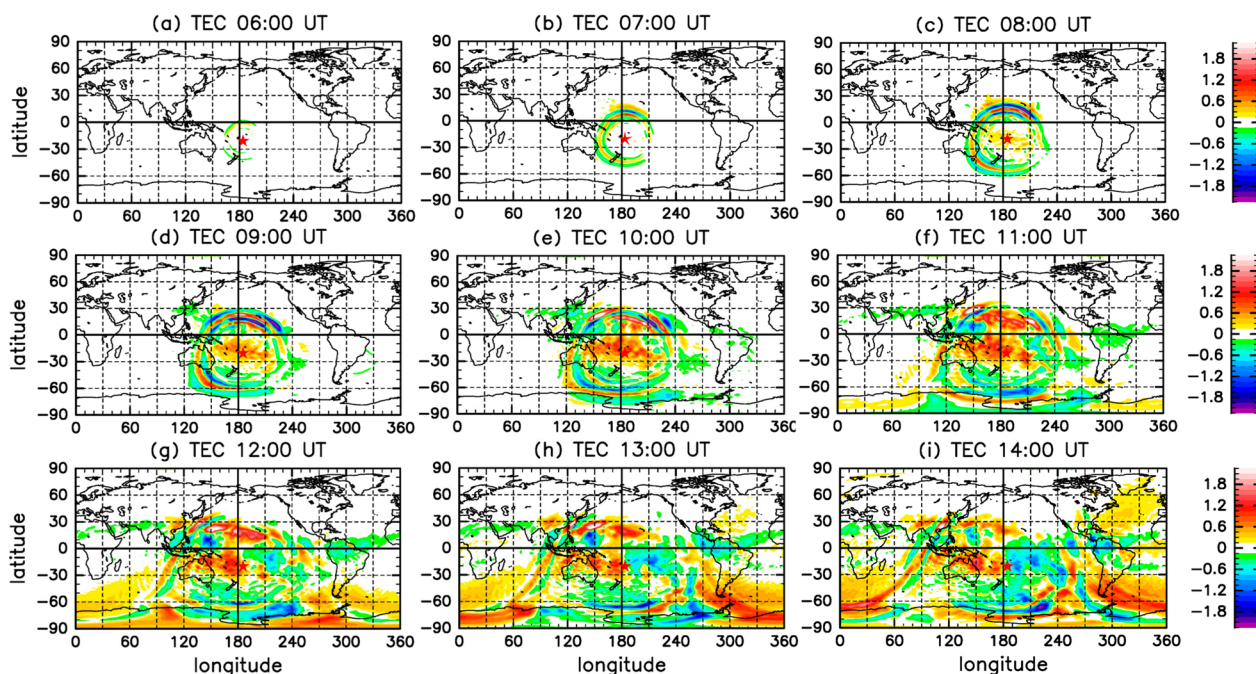
Fig. 1 Global distributions of simulated TEC perturbation triggered by the Hunga-Tonga eruption on 15 January 2022 at 06 UT (**a**), at 07 UT (**b**), at 08 UT (**c**), at 09UT (**d**), at 10 UT (**e**), at 11 UT (**f**), at 12 UT (**g**), at 13 UT (**h**), and 14 UT(**i**). Units are TECU. A red asterisk indicates the location of the Hunga-Tonga volcano. The TEC variation is shown by taking the difference of TEC with and without the Hunga-Tonga eruption

Fig. 2 **a** Latitude–time distribution of simulated TEC perturbation along the 175º W longitude sector on 15 January 2022. Units are TECU. A red asterisk indicates the location of the Hunga-Tonga volcano. The TEC variation is shown byy taking the difference of TEC with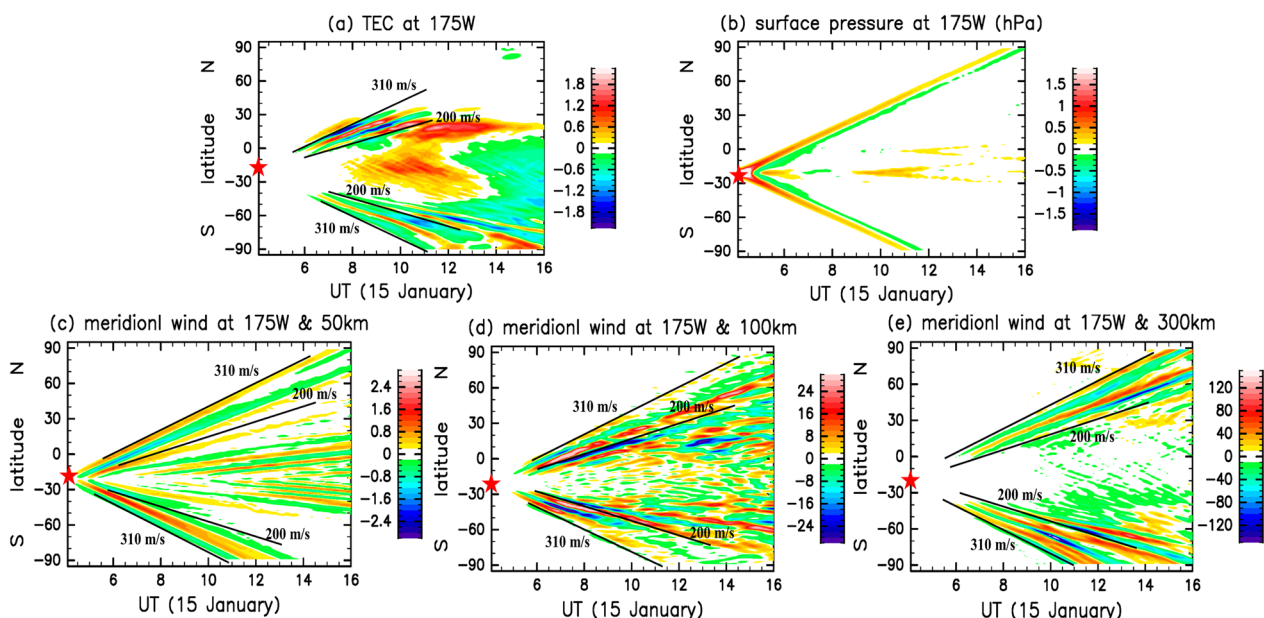 and without the Hunga-Tonga eruption. **b** As in (**a**) but for the surface pressure. Units are hPa. **c** As in (**a**) but for the meridional wind perturbation at 50 km. Units are m/s. **d** As in (**a**) but for the meridional wind perturbation at 100 km. **e** As in (**a**) but for the meridional wind perturbation at 300 km

(e.g., Themens et al. 2022; Zhang et al. 2022; Saito et al., 2022; Shinbori et al. 2022). The first TEC variation travels with a phase speed of about 310 m/s (Fig. 2a), which is similar to the phase speed of the Lamb wave (Fig. 2b). Following the first TEC variation, TEC variations with phase speeds of 200–300 m/s appear (e.g., Zhang et al. 2022).

To investigate the mechanism of the TEC variations, neural wind variations caused by the eruption are examined. Figure 3 shows the global distributions of the meridional wind variations at a height of 300 km (Animation of the meridional wind variation triggered by the Hunga-Tonga eruption is shown in Additional file 3). The meridional wind variations with the amplitude of 50–60 m/s reach over New Zealand at 06 UT, and over Antarctica at 10 UT. The concentric wave structure is clear at 07 UT and 08 UT. The first wind variation due to the concentric wave spreads with a phase speed of 310 m/s (Fig. 2e). After the arrival of the Lamb wave, wind variations with phase speeds of 200–300 m/s appear. These features are similar to those of the TEC variations. The zonal and vertical winds variations at a height of 300 km also have similar features (not shown). These results indicate that the ionospheric perturbations are generated by the neutral wind perturbations via the neutral–plasma interaction process (e.g., Shinagawa et al. 2013; Matsumura et al.

2011). The meridional wind perturbations at 07 UT 08 UT and 10 UT are stronger at 30–70° S than at 0–30° N. As shown in Additional file 1: Figure S2, the northward wind is dominant at 06–08 UT over the equatorial and southern Pacific Ocean. Thus, the enhanced meridional wind variations at 30–70° S are explained by the filtering effect due to the background wind.

The vertical propagation of atmospheric waves from the lower atmosphere is examined here. Figure 4 shows the latitude–height distributions of the meridional wind variations at 06 UT, 08 UT and 10 UT along the 175° W longitude sector. The 175° W longitude sector is chosen, because the Hunga-Tonga volcano is located at 175.4° W. The wind variation associated with the Lamb wave spreads first from the epicenter. The phase front of the Lamb wave is uniform in height. The energy density of the Lamb wave decays with height, so that the wind variation associated with the Lamb wave is small in the thermosphere. After the arrival of the Lamb wave, another type of atmospheric waves appears. The phase fronts at the north (south) of the epicenter slope upward to the north (south). The time evolution of the meridional wind variations shows that the phase line descends with time (Additional file 1: Figure S3), indicative of upward propagating GWs. These structures of the wind variations obtained in this study are quite similar those of triggered by tsunami
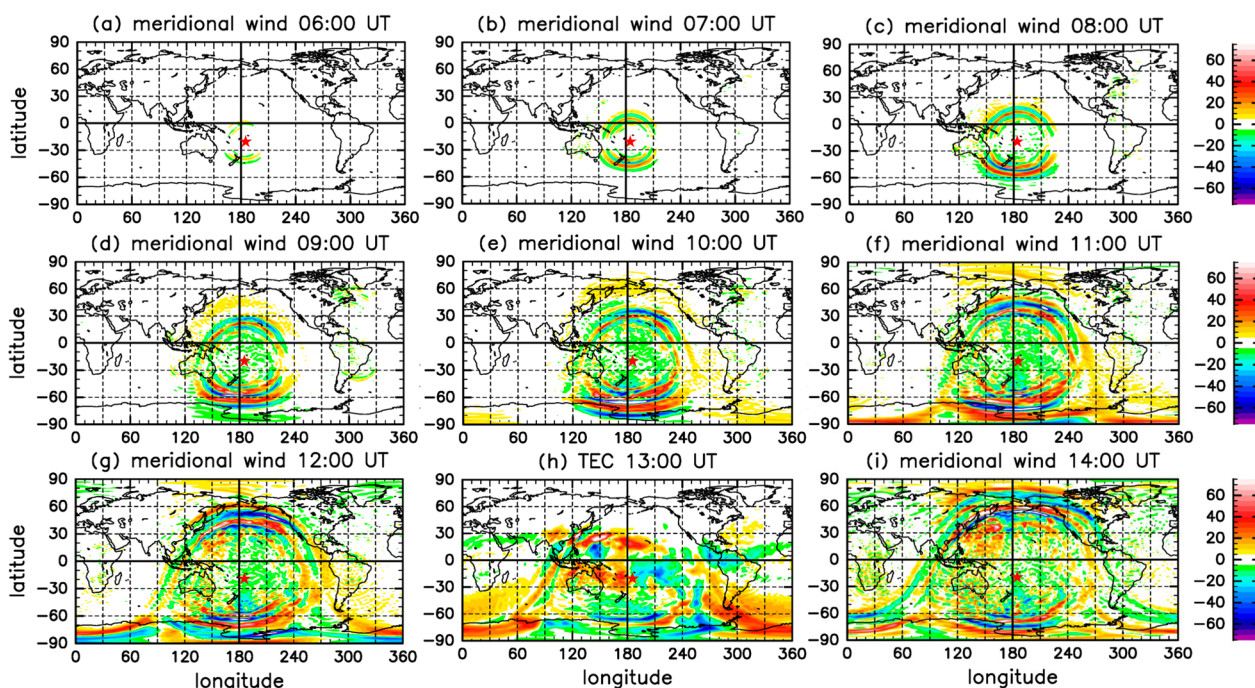

Fig. 3 Global distributions of the simulated meridional wind perturbation at 300 km height triggered by the Hunga-Tonga eruption on 15 January 2022 at 06 UT (**a**), at 07 UT (**b**), at 08 UT (**c**), at 09UT (**d**), at 10 UT (**e**), at 11 UT (**f**), at 12 UT (**g**), at 13 UT (**h**), and 14 UT (**i**). Units are m/s. A red asterisk indicates the location of the Hunga-Tonga volcano. The meridional wind variation is shown by taking the difference of the meridional wind with and without the Hunga-Tonga eruption
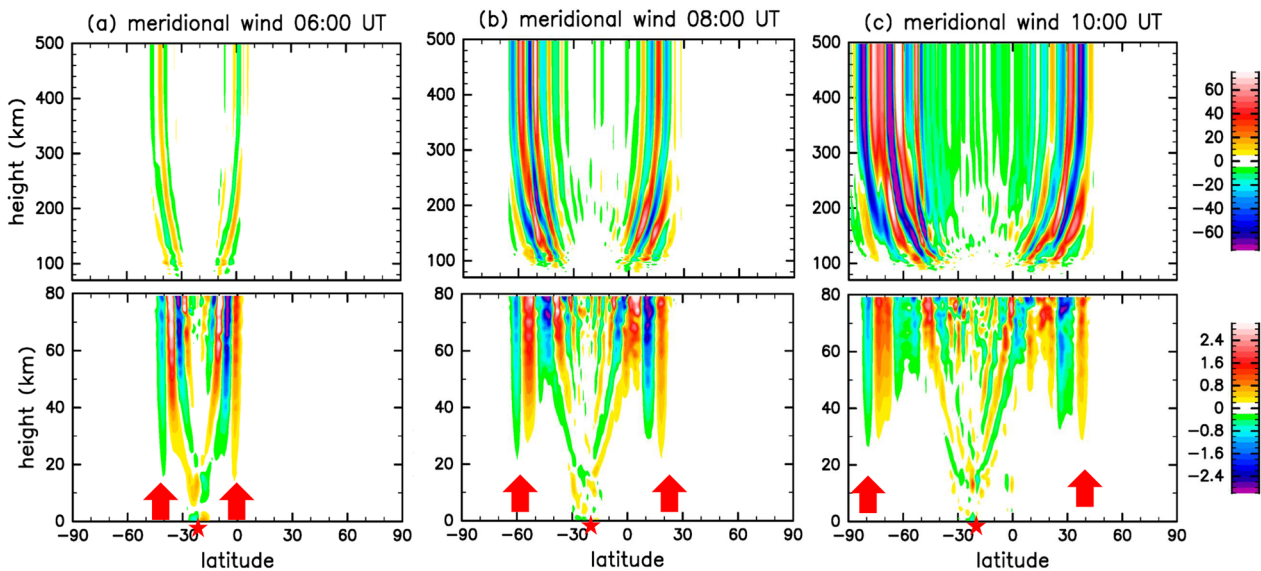
Fig. 4 Height–latitude distribution of the simulated meridional wind perturbation along the 175º E longitude sector on 15 January 2022 at 06 UT (**a**), at 08 UT (**b**), and at 10 UT (**c**). Red arrows indicate the Lamb wave. A red asterisk indicates the location of the Hunga-Tonga volcano. The meridional wind variation is shown by taking the difference of TEC with and without the Hunga-Tonga eruption

(e.g., Laughman et al. 2017; Hickey et al. 2009). The maximum of the GW amplitude occurs just after the arrival of the Lamb wave. The large-amplitude GW was primarily excited by the pressure perturbation imposed at a grid point near the Hunga-Tonga volcano. The GW amplitude is 0.3–0.5,1.0–1.5, 30–40 and 60–80 m/s at heights of 30, 70, 120, and 400 km, respectively. However, wind fluctuations appear intermittently after the first GW (Additional file 1: Figure S3). Figure 3c, d and e shows the latitude-time distribution of the meridional wind variations along the 175º W longitude sector at heights of 50, 100 and 300 km, respectively. At all heights, wind variations with a phase speed of 310 m/s spread from the epicenter. After the first GW, GWs with phase speeds of 200–300 m/s follow.

To investigate the upward propagation of GWs to the thermosphere in more detail, the energy flux associated with GWs are calculated. The upward and meridional energy fluxes associated with GWs are estimated as $\rho v' \varnothing'$, and $\rho w' \varnothing'$, respectively (Miyoshi and Fujiwara 2008). ρ and $\varnothing'$ are density and geopotential fluctuation component, respectively, while v' and w' are meridional and vertical wind fluctuation component, respectively. Figure 5 shows the upward and meridional energy fluxes associated with GWs. The peak of the upward energy flux just after the eruption (04–05 UT) is located in the troposphere near the Hunga-Tonga volcano. The peak of the upward energy flux moves upward with time. Namely, the peak is found at 50–60 km (100–120 km) height at 05–06 UT (06–07 UT). The peak region of the energy flux

moves southward (northward) in the SH (NH). Based on the results obtained in this study, we can conclude that GWs are excited in the troposphere and propagates into the thermosphere. The neutral wind fluctuations caused by upward propagating GWs produce the TEC variations via the neutral–plasma interaction.

Discussion

The present study can reproduce TIDs after the arrival of the Lamb wave. GWs with horizontal phase speeds of 200–310 m/s are excited in the troposphere near the Hunga-Tonga volcano, and propagate upward into the thermosphere. Neutral wind perturbations associated with GWs induce ionospheric variations via the neutral–plasma interaction. However, the TEC variations with phase speeds of 400 and 720 m/s, which are faster than the sound speed in the troposphere, are observed after the Hunga-Tonga eruption (e.g., Themens et al. 2022; Zhang et al. 2022). GAIA cannot simulate acoustic waves, because the model is a hydrostatic model. This result implies that the acoustic wave generated in the troposphere is essential for reproducing the TEC variations with phase speeds faster than the sound speed. Therefore, the present simulation cannot reproduce TEC variations that travels faster than the sound speed. The numerical simulation using a non-hydrostatic model is necessary to simulate these fast TEC variations. This is a subject of the future study. Moreover, Themens et al. (2022) reported TEC variations with horizontal wavelength of 200–500 km. The present study fails to simulate
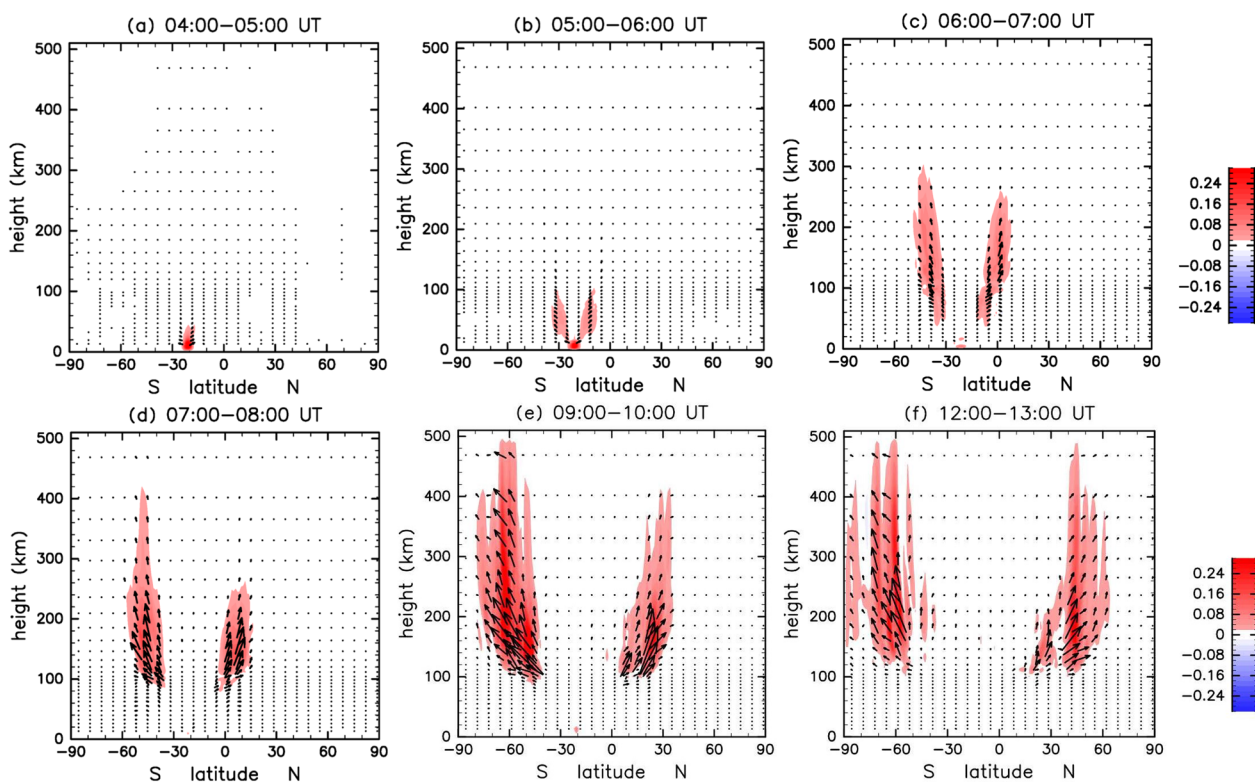
Fig. 5 a Height–latitude distribution of the meridional energy flux associated with GWs averaged a period from 04:00 UT to 05:00 UT (vectors). Color contour indicates the upward energy flux. **b** As in (**a**) but for a period from 05:00 UT to 06:00 UT. **c** As in (**a**) but for a period from 06:00 UT to 07:00 UT. **d** As in (**a**) but for a period from 07:00 UT to 08:00 UT. Units are kgm^{-1}s^{-1}

these TEC variations with horizontal wavelength shorter than 400 km because of the insufficient horizontal resolution of the present model. To simulate TEC variations with horizonal wavelengths of 200–400 km, a numerical model with higher horizontal resolution (∼ 50 km) is required. This is also a subject of the future study.

TEC variations triggered by the eruption appear before the arrival of the Lamb wave. Weak TEC variations occur over the east China sea and Brazil at 09–10 UT, and over Brazil, India and southern China at 10–11 UT. These TEC variations cannot be explained by upward propagation of GWs shown in this study. Saito et al. (2022) and Shinbori et al. (2022) showed that TIDs excited by the eruption was observed over Japan at 07–08 UT. They suggested that TEC/TID variations before the arrival of the Lamb wave are explained by electric field perturbations in the ionosphere. These electric perturbations are generated by neutral wind perturbations in the SH via the E-region dynamo process and are transmitted from the SH to the NH along the magnetic field line (Iyemori et al. 2022; Shinbori et al. 2022). The TEC variations before the arrival of the Lamb wave obtained in this study are probably due to this process. Additional file 1: Figure S4 shows the global distribution of the electric field distribution in

the E-region. At 06 UT, the electric field perturbations driven by the neutral wind perturbations was generated mainly near the Hunga-Tonga volcano, and the electric field perturbations were transmitted to the conjugate points in the northern Pacific Ocean through the interhemispheric electrodynamical coupling. The electric field perturbation at 10 UT spread over Brazil and East Asia. As another prominent feature in TEC variations near the eruption region, Astafyeva et al. (2022) and Aa et al. (2022) observed a strong long-lasting depletion occurred after a large TEC. Such depletion in TEC was not reproduced in our simulation. However, these topics are beyond the scope of the present paper, are subjects of the future study.

Using the MIGHTI instrument on the ICON spacecraft, Harding et al. (2022) investigated the neutral wind perturbations near the wavefront of the Lamb wave. The zonal wind perturbations at 100–150 km height over the north Atlantic Ocean at 14–15 UT exceed 100 m/s, and have the horizontal wavelengths between 3000 and 5000 km, which are not a single wave mode. Additional file 1: Figure S5 shows the height–longitude distribution of the zonal wind perturbations at 35° N simulated in this study. The amplitudes of the wind fluctuations

at 300–400 km are 60–80 m/s. The wave structure is complicated, and does not have a single wave mode. The phase front of the zonal wind perturbations slopes upward to the east. These features of the simulated wind perturbations are quite similar to those of the MIGHTI observation. Our result suggests that the observed wind perturbations are likely due to the GWs triggered by the Hunga-Tonga eruption. However, wind perturbations at 100–150 km are between 30 and 40 m/s, which is smaller than the observation by a factor of 3–4. The simulated horizontal wavelength ranges between 1000–2500 km, which is shorter than the observed wavelength. The number of the wind observation is insufficient to elucidate the relation between the effect of the eruption on the wind perturbations. We need further studies to detect the wind perturbations triggered by the eruption.

Conclusion

Using a global atmosphere–ionosphere coupled model GAIA, for the first time, we showed atmospheric and ionospheric perturbations triggered by the Hunga-Tonga eruption. The features of the simulated TEC variations agree well with those of the TEC observation reported in earlier studies. The main results concerning the mechanism for the observed TEC variation are as follows.

1. The TEC variations are generated by the neutral wind perturbations associated with upward propagating GWs from the troposphere into the thermosphere.
2. GWs with horizontal phase speeds of 200–310 m/s are excited in the troposphere near the Hunga-Tonga volcano, and propagates into the thermosphere. The amplitude of the meridional and zonal wind perturbations due to GWs at 300 km height reaches 60–80 m/s.
3. The eruption-generated GWs whose horizontal phase velocities are close to the sound speed play an important role on variations in the T–I system.

Studies using GNSS(Global Navigation Satellite System)/TEC analysis indicate TIDs propagating faster than the sound speed (e.g., Themens et al. 2022; Lin et al. 2022; Zhang et al. 2022). Since GAIA is not able to simulate acoustic waves, the TIDs that travel faster than the sound speed could not be reproduced. To investigate the fast-TIDs, numerical simulation with a non-hydrostatic model is necessary. This is a subject of the future study. As mentioned before, numerical studies concerning the impact of the Hunga-Tonga eruption with other numerical models are underway, and will be published shortly.

Abbreviations

GAIA	The ground-to-topside of atmosphere and ionosphere for aeronomy
GCM	General circulation model
GNSS	Global navigation satellite system
GW	Gravity wave
NH	Northern hemisphere
SH	Southern hemisphere
TEC	Total electron content
T–I	Thermosphere–ionosphere
TID	Traveling ionospheric disturbance

Supplementary Information

The online version contains supplementary material available at https://doi.org/10.1186/s40623-023-01827-2.

Additional file 1: Figure S1. Height-latitude distribution of the zonal mean temperature on 15 January 2022. Units are K.As inbut for the zonal wind. Units are m/s. Positivevalues indicate eastwardwind. Figure S2.Global distribution of the horizontal windand temperature at 300 km height at 04 UT on 15 January 2022. Units of temperature is K, and units of the wind is m/s. Vectors on the right-hand side indicate the magnitude of 200 m/s.As inbut for at 06 UT.As inbut for at 08 UT. Figure S3.Height–time distribution of the meridional wind perturbation at 175º W longitude and 20º N latitude on 15 January 2022. Units are m/s.As in Figure S4but for at the equator. Figure S4.Global distribution of the eastward Electric field perturbations at 120 km height at 06:00 UT on 15 January 2022. Units are mV/m.As in Figure S5but for 10:00 UT. Figure S5.Height–longitude distribution of the zonal wind perturbations at 35º N at 14:00 UT on 15 January 2022.As inbut for 14:30 UT.As inbut for 15:00 UT.As inbut for 15:30 UT.

Additional file 2: Global distributions of simulated TEC perturbation triggered by the Hunga-Tonga eruption on 15 January 2022. The TEC variation is shown by taking the difference of TEC with and without the Hunga-Tonga eruption.

Additional file 3: Global distributions of the simulated meridional wind perturbation at 300 km height triggered by the Hunga-Tonga eruption on 15 January 2022. Units are m/s. The meridional wind variation is shown by taking the difference of the meridional wind with and without the Hunga-Tonga eruption.

Author contributions

YM conducted numerical simulation and data analysis, and wrote a major part of the manuscript. HS wrote "chapter 1". All authors contributed to discussion on the results and review the manuscript. All authors read and approved the final manuscript.

Availability of data and materials

Please contact Y. Miyoshi for the GAIA model and simulated data. All the data used in this study were obtained from GAIA model.

Declarations

Author details
[1]Department Earth and Planetary Sciences, Faculty of Science, Kyushu University, 744 Motooka Nishiku, Fukuoka 819-0395, Japan. [2]National Institute of Information and Communications Technology, 4-2-1 Nukui-Kitamachi Koganei, Tokyo, Japan.

References

Aa E, Zhang S-R, Erickson PJ, Vierinen J et al (2022) Significant ionospheric hole and equatorial plasma bubbles after the 2022 Tonga volcano eruption. Space Weather 20:e2022SW003101. https://doi.org/10.1029/2022SW003101

Abbrescia M, Avanzini C, Baldini L et al (2022) Observation of Rayleigh-Lamb waves generated by the 2022 Hunga-Tonga volcanic eruption with the POLA detectors at Ny-Ålesund. Sci Rep 12:19978. https://doi.org/10.1038/s41598-022-23984-2

Adam D (2022) Tonga volcano eruption created puzzling ripples in Earth's atmosphere. Nature 601:497. https://doi.org/10.1038/d41586-022-00127-1

Amores A, Monserrat S, Marcos M, Argüeso D, Villalonga J, Jordà G, Gomis D (2022) Numerical simulation of atmospheric Lamb waves generated by the 2022 Hunga-Tonga volcanic eruption. Geophys Res Lett 49:e2022GL098240. https://doi.org/10.1029/2022GL098240

Astafyeva E, Maletckii B, Mikesell TD, Munaibari E, Ravanelli M, Coisson P, Manta F, Rolland L (2022) The 15 January 2022 Hunga Tonga eruption history as inferred from ionospheric observations. Geophys Res Lett 49:e2022GL098827. https://doi.org/10.1029/2022GL098827

Harding BJ, Wu Y-JJ, Alken P, Yamazaki Y, Triplett CC, Immel TJ, Gasque CG, Mende SB, Xiong C (2022) Impacts of the January 2022 Tonga volcanic eruption on the ionospheric dynamo: ICON-MIGHTI and Swarm observations of extreme neutral winds and currents. Geophys Res Lett 49:e2022GL098577. https://doi.org/10.1029/2022GL098577

He J, Astafyeva E, Yue X, Ding F, Maletckii B (2023) The giant ionospheric depletion on 15 January 2022 around the Hunga Tonga-Hunga Ha'apai volcanic eruption. J Geophys Res Space Phys 128:e2022JA030984. https://doi.org/10.1029/2022JA030984

Heki K (2022) Ionospheric signatures of repeated passages of atmospheric waves by the 2022 Jan 15 Hunga Tonga-Hunga Ha'apai eruption detected by QZSS-TEC observations in Japan. Earth Planets Space 74:112. https://doi.org/10.1186/s40623-022-01674-7

Hickey MP, Schubert G, Walterscheid RL (2009) Propagation of tsunami-driven gravity waves into the thermosphere and ionosphere. J Geophys Res 114:A08304. https://doi.org/10.1029/2009JA014105

Iyemori T, Nishioka M, Otsuka Y, Shinbori A (2022) A confirmation of vertical acoustic resonance and field-aligned current generation just after the 2022 Hunga Tonga Hunga Ha'apai volcanic eruption. Earth Planets Space 74:103. https://doi.org/10.1186/s40623-022-01653-y

Jin H, Miyoshi Y, Fujiwara H, Shinagawa H (2008) Electrodynamics of the formation of ionospheric wave number 4 longitudinal structure. J Geophys Res 113:A09307. https://doi.org/10.1029/2008JA013301

Jin H, Miyoshi Y, Fujiwara H, Shinagawa H, Terada K, Terada N, Ishii M, Otsuka Y, Saito A (2011) Vertical connection from the tropospheric activities to the ionospheric longitudinal structure simulated by a new Earth's whole atmosphere-ionosphere coupled model. J Geophys Res 116:A01316. https://doi.org/10.1029/2010JA015925

Jin H, Miyoshi Y, Pancheva D, Mukhtarov P, Fujiwara H, Shinagawa H (2012) Response of migrating tides to the stratospheric suden warming in 2009 and their effects on the ionosphere studied by a whole atmosphere-ionosphere model GAIA with COSMIC and TIMED/SABER observations. J Geophys Res 117:A10323. https://doi.org/10.1029/2012JA017650

Kobayashi S, Ota Y, Harada Y, Ebita A, Moriya M, Onoda H, Onogi K, Kamahori H, Kobayashi C, Endo H, Miyaoka K, Takahashi K (2015) The JRA-55 Reanalysis: General specifications and basic characteristics. J Meteor Soc Japan 93:5–48. https://doi.org/10.2151/jmsj.2015-001

Kubo H, Kubota T, Suzuki W et al (2022) Ocean-wave phenomenon around Japan due to the 2022 Tonga eruption observed by the wide and dense ocean-bottom pressure gauge networks. Earth Planets Space 74:104. https://doi.org/10.1186/s40623-022-01663-w

Laughman B, Fritts DC, Lund TS (2017) Tsunami-driven gravity waves in the presence of vertically varying background and tidal wind structures. J Geophys Res Atmos 122:5076–5096. https://doi.org/10.1002/2016JD025673

Lin J-T, Rajesh PK, Lin CH, Chou M-Y, Liu J-Y, Yue J, Tsai H-F, Chao H-M, Kung M-M (2022) Rapid conjugate appearance of the giant ionospheric lamb wave in the northern hemisphere after Hunga-Tonga Volcano Eruptions. ESS Open Archive. https://doi.org/10.1002/essoar.10510440.2

Matoza RS et al (2022) Atmospheric waves and global seismoacoustic observations of the January 2022 Hunga eruption, Tonga. Science. https://doi.org/10.1126/science.abo7063

Matsumura M, Saito A, Iyemori T, Shinagawa H, Tsugawa T, Otsuka Y, Nishioka M, Chen CH (2011) Numerical simulations of atmospheric waves excited by the 2011 off the Pacific coast of Tohoku Earthquake. Earth Planet Space 63:68. https://doi.org/10.5047/eps.2011.07.015

Miyoshi Y, Fujiwara H (2003) Day-to-day variations of migrating diurnal tide simulated by a GCM from the ground surface to the exobase. Geophys Res Lett 30(15):1789. https://doi.org/10.1029/2003GL017695

Miyoshi Y, Fujiwara H (2006) Excitation mechanism of intraseasonal oscillation in the equatorial mesosphere and lower thermosphere. J Geophys Res 111:D14108. https://doi.org/10.1029/2005JD006993

Miyoshi Y, Fujiwara H (2008) Gravity waves in the thermosphere simulated by a general circulation model. J Geophys Res 113:D01101. https://doi.org/10.1029/2007JD008874

Miyoshi Y, Yamazaki Y (2020) Excitation mechanism of ionospheric 6-day oscillation during the 2019 September sudden stratospheric warming event. J J Geophys Res 125:e2020JA028283. https://doi.org/10.1029/2020JA028283

Miyoshi Y, Jin H, Fujiwara H, Shinagawa H (2018) Numerical studyof traveling ionospheric disturbances generated by an upward propagating gravity wave. J Geophys Res. https://doi.org/10.1002/2017JA025110

Saito S (2022) Ionospheric disturbances observed over Japan following the eruption of Hunga Tonga-Hunga Ha'apai on 15 January 2022. Earth Planet Space 74:57. https://doi.org/10.1186/s40623-022-01619-0

Shinagawa H (2009) Ionosphere simulation. J Natl Inst Infor Commun Technol 56:199–207

Shinagawa H, Tsugawa T, Matsumura M, Iyemori T, Saito A, Maruyama T, Jin H, Nishioka M, Otsuka Y (2013) Two-dimensional simulation of ionospheric variations in the vicinity of the epicenter of the Tohoku-oki earthquake on 11 March 2011. Geophys Res Lett 40:5009–5013. https://doi.org/10.1002/2013GL057627

Shinbori A, Otsuka Y, Sori T, Nishioka M, Perwitasari S, Tsuda T, Nishitani N (2022) Electromagnetic conjugacy of ionospheric disturbances after the 2022 Hunga Tonga-Hunga Ha'apai volcanic eruption as seen in GNSS-TEC and SUperDARN Hokkaido pair of radars observations. Earth Planets Space 74:106. https://doi.org/10.1186/s40623-022-01665-8

Themens DR, Watson C, Žagar N, Vasylkevych S, Elvidge S, McCaffrey A, Prikryl P, Reid B, Wood A, Jayachandran P (2022) Global propagation of ionospheric disturbances associated with the 2022 Tonga volcanic eruption. Geophys Res Lett 49:e2022GL098158. https://doi.org/10.1029/2022GL098158

Yamada M, Ho T-C, Mori J, Nishikawa Y, Yamamoto M-Y (2022) Tsunami triggered by the Lamb wave from the 2022 Tonga volcanic eruption and transition in the offshore Japan region. Geophys Res Lett 49:e2022GL098752. https://doi.org/10.1029/2022GL098752

Yamazaki Y, Soares G, Matzka J (2022) Geomagnetic detection of the atmospheric acoustic resonance at 38 mHz during the Hunga Tonga eruption event on 15 January 2022. J Geophys Res Space Phys 127:e2022JA030540. https://doi.org/10.1029/2022JA030540

Zhang S-R, Vierinen J, Aa E, Goncharenko LP, Erickson PJ, Rideout W, Coster AJ, Spicher A (2022) Tonga volcanic eruption induced global propagation of ionospheric disturbances via lamb waves. Front Astron Space Sci 9:871275. https://doi.org/10.3389/fspas.2022.871275

Publisher's Note